

Statistical Correlation Between Quantum Entanglement and Spin–Orbit Coupling in Crossed Beam Molecular Dynamics

Junxu Li, Manas Sajjan, Sumit Suresh Kale, and Sabre Kais*

Non-classical features like interference are already being harnessed to control the output of chemical reactions. However, quantum entanglement which is an equally enigmatic many-body quantum correlation can also be used as a powerful resource yet has eluded explicit attention. In this report, an experimental scheme under the crossed beam molecular dynamical setup, with the $F + HD$ reaction, is proposed aiming to study the possible influence of entanglement within reactant pairs on the angular features of the product distribution. The aforesaid reaction has garnered interest recently, as an unusual horseshoe shape pattern in the product (HF) distribution was observed, which has been attributed to the coupling of spin and orbital degrees of freedom. An experimental scheme is proposed aiming to study the possible influence of entanglement on the necessity for the inclusion of such spin–orbit characteristics, under circumstances wherein the existence of entanglement and spin–orbit interaction is simultaneously detectable. The attainable results are further numerically simulated highlighting specific patterns corresponding to various possibilities. Such studies if extended can provide unforeseen mechanistic insight into analogous reactions, too, from the lens of quantum information.

tools,^[5–7] and even to unravel the mysteries of complex chemical processes by precisely simulating large chemical systems.^[8–10]

Entanglement is a distinctive quantum mechanical feature that represents a strong correlation in many-body systems unexplainable by classical physics. It exists at the core of quantum information processing and may prove essential for quantum speed-up.^[11] Several experiments realized entanglement in a wide range of physical systems, including trapped ions,^[12] quantum dots,^[13] superconducting qubits,^[14] photons,^[15] between an atom and a molecule^[16,17] and in complex chemical and biological systems.^[18–21] The coherent control of chemical reactions has been a long withstanding challenge in chemical physics and several studies have already found new powerful techniques that employ quantum superposition and interference to resolve this issue.^[22–24] However, entanglement as a resource has received scanty attention so far. In this report, we serve to address this lacuna and

focus on gaining a deep insight on the correlations between pre-existing entanglement in a chemical reaction and how it affect the geometrical distribution of product formation.

We choose to elucidate the implications using the $F + H_2$ reaction as a test-bed. Such a choice is motivated by the fact that in the domain of resonances in chemical reactions, the $F + H_2$ system, together with its said isotopic partner has been used to benchmark many studies.^[25–29] Theoretical calculations first predicted the existence of reactive resonances for the $F + H_2$ reaction in 1973 using the collinear reaction model.^[30,31] Though such short-lived reactive resonance in the transition state of chemical reactions has been long predicted based on quantum dynamics simulations,^[32] the direct characterization of transition states has been in the past a grand challenge in physical chemistry,^[33,34] due to the experimental absence of the characteristic Lorentzian signatures in the integral cross section (ICS).^[35] However, in 1984, the forward-scattering peak potentially attributable to the reactive resonances for $HF(v' = 3)$ was first observed by Lee and co-workers in a crossed-molecular beam experiment performed on the $F + H_2$ reactions.^[36] Even though the study was pioneering, yet the assertions remained inconclusive due to possible existence of other dynamical origins for the forward scattering peak.^[37,38] To locate the reactive resonance, techniques of transition-state spectroscopy were later

1. Introduction

The past decades have seen tremendous progress in the field of quantum information and quantum computing. With the expeditious developments in the hardware and software fronts, the algorithms developed on current state-of-the-art quantum computers could help us to overcome the research obstacles that are beyond the capacity of the best available supercomputers.^[1,2] The veritable workhorse of such algorithms are fundamental quantum properties such as superposition, entanglement, coherence, and interference which have been aptly exploited in secure communication,^[3,4] to develop better sensing and meteorological

J. Li, M. Sajjan, S. S. Kale, S. Kais
Department of Chemistry
Department of Physics and Astronomy
Purdue Quantum Science and Engineering Institute
Purdue University
West Lafayette, IN 47907, USA
E-mail: kais@purdue.edu

 The ORCID identification number(s) for the author(s) of this article can be found under <https://doi.org/10.1002/qute.202100098>

DOI: 10.1002/qute.202100098

employed probing the dynamics near the transition state via the negative ion (FH_2^-) photodetachment study.^[39,40]

The controversies of this scattering peak were finally resolved at the beginning of 21st century with the isotopic analogous reaction $\text{F} + \text{HD}$.^[35] In the next two decades, enormous enthusiasm was evoked investigating both the $\text{F} + \text{H}_2$ and $\text{F} + \text{HD}$ reactions using various advanced technologies, such as the negative-ion photodetachment spectroscopic method,^[41,42] and the highly sensitive H atom Rydberg tagging time-of-flight method,^[43–45] even though in all the above studies, the experimental signature could be accurately explained based on the adiabatic theory thereby obviating the need to include special characteristics like the spin–orbit coupling. The situation however changed recently when a peculiar horseshoe-shaped pattern was observed in the product rotational-state–resolved differential cross section (DCS) in $\text{F}(^2P_{3/2}) + \text{HD}$ reactions, which the authors attribute to full spin–orbit characteristics.^[46] The remarkably unusual dynamical pattern provides a window into studying how the spin–orbit interaction can effectively influence chemical reactions. Intuitively, there arises a question whether the pre-existence of entanglement between the reacting partners would have any influence on the spin–orbit interaction in the $\text{F} + \text{HD}$ reaction. For instance, what if the incident F atoms are entangled pairs between the ground state $^2P_{3/2}$ and the excited state $^2P_{1/2}$. Though the pioneers have already considered the inclusion of entanglement in chemical reactions,^[47,48] the possible correlation it may share with spin–orbit coupling have not been explicated as it is an inherently challenging study. As a simple example, if we prepare a number of entangled F atom pairs dividing into two groups, then estimating the entanglement witness function measuring one group, while studying the chemical reactions using the other one, the result can hardly be convincing due to the possibility that entanglement might get broken in collision. Thus, one must ensure that the spin–orbit interaction and entanglement can be detected simultaneously. In this paper, we will propose a scheme for the simultaneous detection of spin–orbit characteristics and entanglement in the $\text{F} + \text{HD} \rightarrow \text{HF} + \text{D}$ reactions.

The organization of the paper is as follows. In Section 2, we propose the experimental setup and discuss the implementation thoroughly. In Section 2.1, we review the need for the inclusion of spin–orbit coupling as illustrated in ref. [46]. In Section 2.2, we elucidate how correlations due to entanglement between the initial pair of F may be experimentally revealed and quantified. In Section 3, we simulate and analyze the various outcomes of the proposed experiment. We conclude thereafter with possible future implications.

2. Experimental Design

The objective of the experiment is to detect entanglement in the prepared atom pairs, and further study if the existence of entanglement would effect the spin–orbit interactions in the transition state. In the following discussions and simulations, we denote the ground state of F ($^2P_{3/2}$) as $|0\rangle$ state and the excited state ($^2P_{1/2}$) as $|1\rangle$ state, which are eigenstates of Pauli Z measurement. Additionally, $|+\rangle = \frac{1}{\sqrt{2}}(|0\rangle + |1\rangle)$ and $|-\rangle = \frac{1}{\sqrt{2}}(|0\rangle - |1\rangle)$ are eigenstates of Pauli X measurement. Scheme of the experi-

mental design is shown as **Figure 1**. Initially, two F atoms are prepared at some certain states, such as Bell state for maximum entanglement, mixed states, superposition states, or Werner states. The atom pair will then be separated into two channels as shown in Figure 1b,c. In the first channel, the single F atom is sent into the scattering chamber together with a beam of HD ($\nu = 0, j = 0$) molecules. If the F atom collides with the beam, a charge-coupled device (CCD) camera will capture and record the image, based on which the differential scattering cross-section (DCS) can be obtained. The scattering process corresponds to measurement Z with eigenstate $|0\rangle$ and $|1\rangle$, while the F atom that does not collide with the HD beam will be measured under measurement X. The blue cylinder in Figure 1b represents a sensor applying. In the other channel, the scattering process corresponds to measurement $\frac{Z+X}{\sqrt{2}}$, while measurement $\frac{Z-X}{\sqrt{2}}$ will be applied on the atom that avoided the collision. Figure 1d is a sketch of the reaction $\text{F} + \text{HD} \rightarrow \text{HF} + \text{D}$. The F atom (green) and HD molecule (blue and purple) will form a transition state when collision happens and then get scattered into the HF (ν', j') (green and blue) molecule and D atom (purple).

2.1. Necessity for Inclusion of Spin–Orbit Coupling

The $\text{F} + \text{HD}(\nu = 0, j = 0)$ reaction shown in Figure 1d will be studied by using a crossed molecular beam (CMB) apparatus with an ion imaging detector.^[49] In the D-atom product velocity map image from $\text{F}(^2P_{3/2}) + \text{HD}(\nu = 0, j = 0)$ reaction,^[46] there are two main ring structures indicating the HF products with vibrational states $\nu' = 2$ or $\nu' = 3$. While the $\nu' = 3$ products are mainly forward scattered, most $\nu' = 2$ products are backward scattered with substantial forward and sideways scatterings. Particularly, unusual horseshoe-shaped structures are detected in the forward-scattering hemisphere around peaked angular distributions of $\nu' = 2$ products in different j' states.^[46] Theoretically, the reactive scattering can be calculated with the coupled two state model or the full six-state model. The Hamiltonian in Jacobi coordinate could be written as^[50]

$$H = -\frac{\hbar^2}{2\mu_R} \frac{\partial^2}{\partial R^2} - \frac{\hbar^2}{2\mu_r} \frac{\partial^2}{\partial r^2} + \frac{L^2}{2\mu_R R^2} + \frac{j^2}{2\mu_r r^2} + V \quad (1)$$

where μ_R is the reduced mass between the center of mass of F and HD molecule, R is the length of the vector \mathbf{R} pointing from F atom to the HD center of mass, μ_r is the reduced mass of HD, and r is the HD bond length. Moreover, j is the rotational angular momentum, and L is the operator for the orbital end-over-end angular momentum of the atom around the center of mass of the diatomic. In the coupled two state model, the F atoms are treated as structureless particles, where both the electron spin (\mathbf{s}) and the electron orbital angular momentum (\mathbf{l}) are neglected. Then potential energy V under the coupled two state model can be written as^[50]

$$V = \begin{pmatrix} V_\Sigma & -\sqrt{2}B \\ -\sqrt{2}B & A + V_\Pi \end{pmatrix} \quad (2)$$

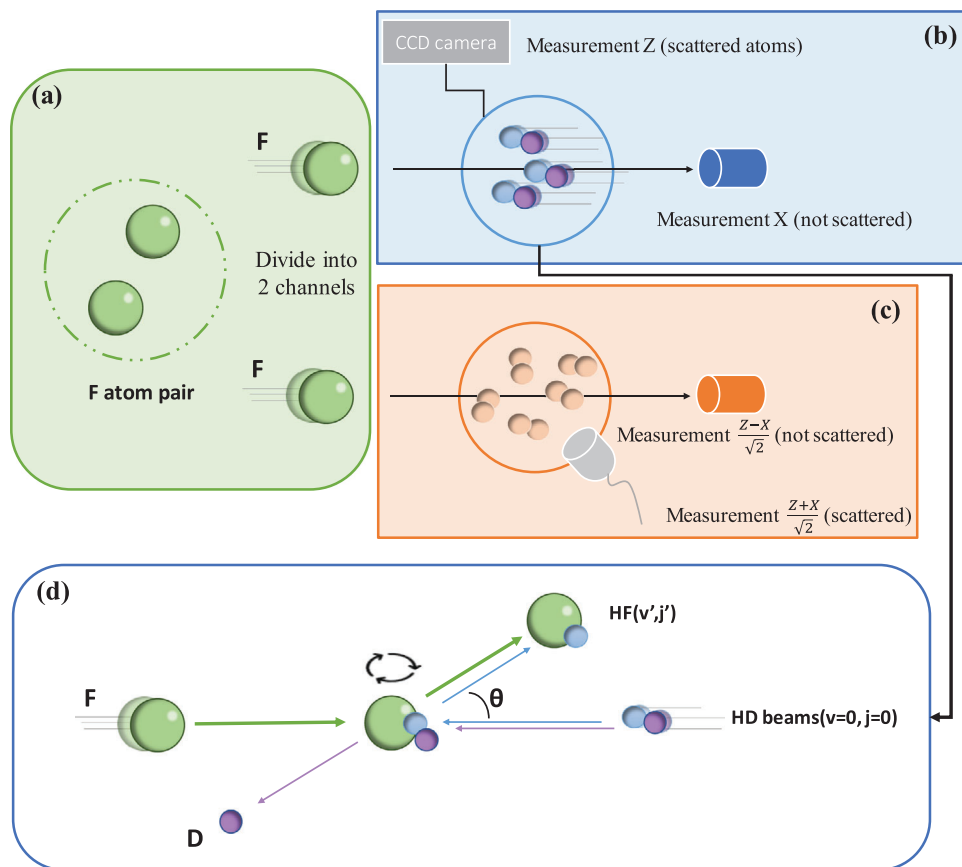


Figure 1. Scheme of the experiment setting. a) A pair of F atoms are prepared at some certain states initially. They are then separated for two channels as shown in (b) and (c). b) In the first channel, the single F atom is sent into the scattering chamber together with a beam of HD ($\nu = 0, j = 0$) molecules. If the F atom collides with the beam, a charge-coupled device (CCD) camera will capture and record the image, based on which the differential scattering cross-section can be derived. The scattering process corresponds to measurement Z with eigenstate $|0\rangle$ and $|1\rangle$. The blue cylinder represents is sensor, where the F atom that does not collide with the HD beam will be measured under measurement X with eigenstate $|+\rangle$ and $|-\rangle$. c) In the second channel, F atom is sent to another scattering chamber. The scattering process corresponds to measurement $\frac{Z+X}{\sqrt{2}}$, while measurement $\frac{Z-X}{\sqrt{2}}$ will be applied on the atom that avoided collision. d) Sketch of the collision between F atom (green) and HD ($\nu = 0, j = 0$) molecule (blue, purple). θ represents the scattering angle between the HD beam and the HF(ν', j') molecule.

where the matrix elements A and B describe the usual spin-orbit couplings, V_Σ, V_Π are determined by the ab initio calculations. In a Cartesian basis, $V_\Sigma = V_{zz}, V_\Pi = (V_{xx} + V_{yy})/2$.

On the other hand, in the full six-state model including the open-shell characteristics of F atoms, V in Equation (1) represents the potential energy surface (PES) containing two components $V = V_{el} + V_{so}$. V_{el} is the adiabatic potential energy surfaces for specific electronic states and nonadiabatic coupling terms, while V_{so} is the electrostatic spin-orbit coupling term, each of which can be written as a 6×6 matrix, and can be written as^[50,51]

$$V_{el} = \begin{matrix} & |\Sigma\rangle & |\bar{\Sigma}\rangle & |\Pi_1\rangle & |\bar{\Pi}_1\rangle & |\Pi_{-1}\rangle & |\bar{\Pi}_{-1}\rangle \\ \begin{matrix} |\Sigma\rangle \\ |\bar{\Sigma}\rangle \\ |\Pi_1\rangle \\ |\bar{\Pi}_1\rangle \\ |\Pi_{-1}\rangle \\ |\bar{\Pi}_{-1}\rangle \end{matrix} & \begin{pmatrix} V_\Sigma & 0 & -V_1 & 0 & V_1 & 0 \\ 0 & V_\Sigma & 0 & -V_1 & 0 & V_1 \\ -V_1 & 0 & V_\Pi & 0 & V_2 & 0 \\ 0 & -V_1 & 0 & V_\Pi & 0 & V_2 \\ V_1 & 0 & V_2 & 0 & V_\Pi & 0 \\ 0 & V_1 & 0 & V_2 & 0 & V_\Pi \end{pmatrix} \end{matrix} \quad (3)$$

$$V_{so} = \begin{matrix} & |\Sigma\rangle & |\bar{\Sigma}\rangle & |\Pi_1\rangle & |\bar{\Pi}_1\rangle & |\Pi_{-1}\rangle & |\bar{\Pi}_{-1}\rangle \\ \begin{matrix} |\Sigma\rangle \\ |\bar{\Sigma}\rangle \\ |\Pi_1\rangle \\ |\bar{\Pi}_1\rangle \\ |\Pi_{-1}\rangle \\ |\bar{\Pi}_{-1}\rangle \end{matrix} & \begin{pmatrix} 0 & 0 & 0 & -\sqrt{2}B & 0 & 0 \\ 0 & 0 & 0 & 0 & -\sqrt{2}B & 0 \\ 0 & 0 & -A & 0 & 0 & 0 \\ -\sqrt{2}B & 0 & 0 & A & 0 & 0 \\ 0 & -\sqrt{2}B & 0 & 0 & A & 0 \\ 0 & 0 & 0 & 0 & 0 & -A \end{pmatrix} \end{matrix} \quad (4)$$

Similarly to $V_\Sigma, V_\Pi, V_1, V_2$ are also determined by the ab initio calculation as $V_1 = V_{xz}/\sqrt{2}, V_2 = (V_{yy} - V_{xx})/2$.

Theoretically calculated DCS for product HF($\nu' = 2, j' = 5$)^[46] with these two models are shown in Figure 2a,b. Two-state coupling model leads to three peaks around the forward-scattering direction, instead of the horseshoe shape pattern. The DCS from full six-state model fits the experiment results very well, while the two-state coupling model cannot explain the unusual horseshoe shape signature, indicating that the full spin-orbit effects are essential to explain the F + HD reaction.^[46] Thus, the

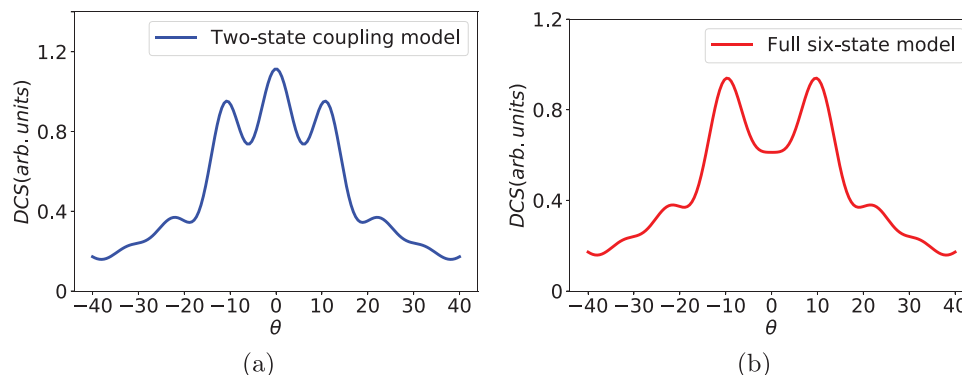


Figure 2. Theoretically calculated DCSs for product HF ($\nu' = 2, j' = 5$) around the forward-scattering direction in the F + HD reaction. a) Theoretically calculated DCS based on two-state coupling model, where the F atoms are treated as structureless particles. Three peaks arise around the forward-scattering direction. b) Theoretically calculated DCS based on full six-state model, where full spin-orbit effects are included. The theoretical DCSs fit well with the horseshoe shape pattern observed in experiments.^[46] In both figures, θ is the scattering angle, and collision energy is around $2.10 \text{ kcal mol}^{-1}$.

horseshoe pattern in F + HD reaction is reliable evidence for the spin-orbit characteristic.

2.2. Detection of Entanglement

As shown in Figure 1b,c, there are two scattering processes and two direct measurements on the unscattered particles in each channel. Two scattering processes correspond to the measurement Z and measurement $\frac{Z+X}{\sqrt{2}}$, while measurement X and $\frac{Z-X}{\sqrt{2}}$ are applied on the unscattered particles. All four measurements together implement a Clauser-Horne-Shimony-Holt (CHSH) experiment^[52] detecting the existence of entanglement. Generally, the CHSH inequality can be written as

$$|E(r_1, t_1) - E(r_1, t_2) + E(r_2, t_1) + E(r_2, t_2)| \leq 2 \quad (5)$$

where the variables r_i and $t_i \forall i$ encode the respective outcomes of the two measurement observables (\tilde{r}, \tilde{t}). $E(r_i, t_i)$ is a measure of quantum correlation in the results obtained from a pair of such outcomes. In the standard Bell test or CHSH experiment, all the four measurements lead to binary values, that is, $\{r_i, t_i\} \in \{+, -\}$. The measure of quantum correlation $E(r_i, t_i)$ in such a case is definable as

$$E(r, t) = \frac{N_{++} - N_{+-} - N_{-+} + N_{--}}{N_{++} + N_{+-} + N_{-+} + N_{--}} \quad (6)$$

where N_{++} represents the number of particle pairs yielding result $+$ in both the measurement of observable \tilde{r} of channel I and measurement of observable \tilde{t} of channel II. The four $E(r_i, t_i)$ terms form the test statistics parameter $S = E(r_1, t_1) - E(r_1, t_2) + E(r_2, t_1) + E(r_2, t_2)$.

However, in the experiment shown in Figure 1, chemical reactions are included, which leads to continuous measurement outcomes. Thus, Equation (6), the standard definition of quantum correlations in Bell test, no longer works in such a scattering process. For chemical reactions, instead, the generalized CHSH inequality for continuous variables^[53] is required. We denote $M(\mathbf{x}_1, \mathbf{x}_2 | \rho, \tilde{r}, \tilde{t}) d\mathbf{x}_2 d\mathbf{x}_1$ as the probability to get a measurement outcome within volume $d\mathbf{x}_1$ centered at \mathbf{x}_1 under observable \tilde{r} and

within volume $d\mathbf{x}_2$ centered at \mathbf{x}_2 under observable \tilde{t} for a particle pair with density matrix ρ . We always have $M(\mathbf{x}_1, \mathbf{x}_2 | \rho, \tilde{r}, \tilde{t}) \geq 0$ and $\int d\mathbf{x}_1 d\mathbf{x}_2 M(\mathbf{x}_1, \mathbf{x}_2 | \rho, \tilde{r}, \tilde{t}) = 1$. Similarly, we denote $M(\mathbf{x}_1 | \rho', \tilde{r})$ as the marginal probability density to get measurement result in the neighborhood of \mathbf{x}_1 under measurement observable \tilde{r} irrespective of the outcome of the observable \tilde{t} for a single particle with density matrix ρ' . Let us define an auxiliary function for the outcome measurement \tilde{r} and \tilde{t} as^[53]

$$V(\mathbf{x}_1, \mathbf{x}_2 | \tilde{r}, \tilde{t}) = [\nu(\mathbf{x}_1 | +, \tilde{r}) - \nu(\mathbf{x}_1 | -, \tilde{r})] \cdot [\nu(\mathbf{x}_2 | +, \tilde{t}) - \nu(\mathbf{x}_2 | -, \tilde{t})] \quad (7)$$

and $\nu(\mathbf{x} | \pm, \tilde{r})$ are defined as

$$\nu(\mathbf{x} | \pm, \tilde{r}) = \frac{\left[\begin{array}{l} M(\mathbf{x} | \phi_r^\pm) \langle \phi_r^\pm |, \tilde{r} \rangle \\ - \int d\mathbf{x}' M(\mathbf{x}' | \phi_r^\pm) \langle \phi_r^\pm |, \tilde{r} \rangle M(\mathbf{x} | \phi_r^\mp) \langle \phi_r^\mp |, \tilde{r} \rangle \end{array} \right]}{\left[\begin{array}{l} \int d\mathbf{x}' M(\mathbf{x}' | \phi_r^\pm) \langle \phi_r^\pm |, \tilde{r} \rangle M(\mathbf{x} | \phi_r^\pm) \langle \phi_r^\pm |, \tilde{r} \rangle \\ - \int d\mathbf{x}' M(\mathbf{x}' | \phi_r^\pm) \langle \phi_r^\pm |, \tilde{r} \rangle M(\mathbf{x} | \phi_r^\mp) \langle \phi_r^\mp |, \tilde{r} \rangle \end{array} \right]} \quad (8)$$

where $|\phi_r^\pm\rangle$ represent the two eigenstates corresponding to values $\{+, -\}$ in measurement of \tilde{r} . Similar considerations applies to \tilde{t} -measurement as well. Then we get the generalized CHSH inequality for continuous variables taking the following form

$$\left| \int d\mathbf{x}_1 d\mathbf{x}_2 M(\mathbf{x}_1, \mathbf{x}_2 | \rho, \tilde{r}_1, \tilde{t}_1) V(\mathbf{x}_1, \mathbf{x}_2 | \tilde{r}_1, \tilde{t}_1) - \int d\mathbf{x}_1 d\mathbf{x}_2 M(\mathbf{x}_1, \mathbf{x}_2 | \rho, \tilde{r}_1, \tilde{t}_2) V(\mathbf{x}_1, \mathbf{x}_2 | \tilde{r}_1, \tilde{t}_2) + \int d\mathbf{x}_1 d\mathbf{x}_2 M(\mathbf{x}_1, \mathbf{x}_2 | \rho, \tilde{r}_2, \tilde{t}_1) V(\mathbf{x}_1, \mathbf{x}_2 | \tilde{r}_2, \tilde{t}_1) + \int d\mathbf{x}_1 d\mathbf{x}_2 M(\mathbf{x}_1, \mathbf{x}_2 | \rho, \tilde{r}_2, \tilde{t}_2) V(\mathbf{x}_1, \mathbf{x}_2 | \tilde{r}_2, \tilde{t}_2) \right| \leq 2 \quad (9)$$

More discussion about the detection of entanglement in chemical reactions can be found in our recent work.^[53]

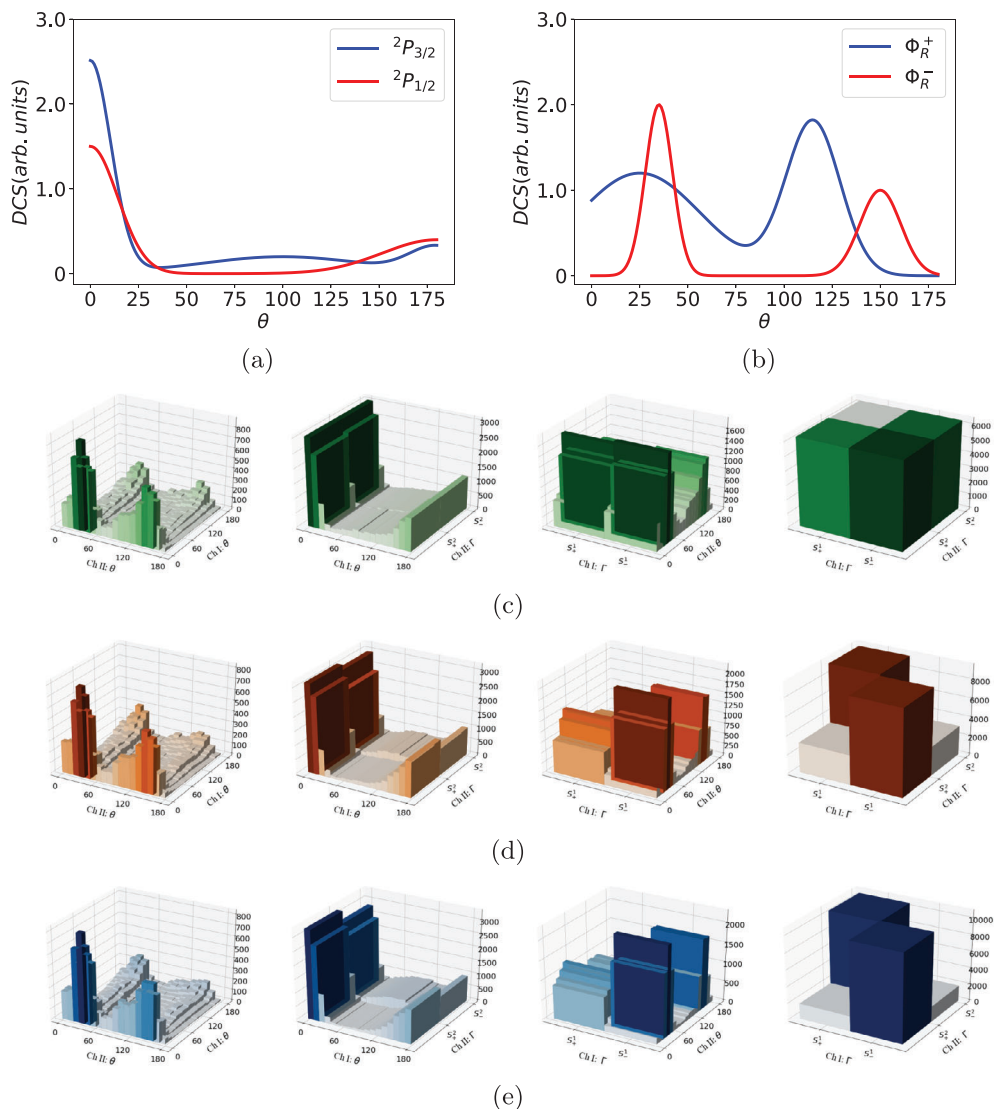


Figure 3. DCSs for the reactions and numerical simulations for various Werner states. a) Scheme of the DCS for the $F(^2P_{1/2,3/2}) + HD(\nu = 0, j = 0)$ reaction, only the HF($\nu' = 3$) product is included. b) DCS of $|\Phi_R^\pm\rangle$ in the reaction corresponding to measurement $\frac{Z+X}{\sqrt{2}}$, where $|\Phi_R^\pm\rangle$ are eigenstates of $\frac{Z+X}{\sqrt{2}}$. c–e) Numerical simulations for Werner states with various p values $p = 0, 0.707, 1$. Histograms represent the count of F atom pairs with certain measurement results, where θ is the scattering angle of product HF($\nu' = 3$), and Γ is the direct measurement result with two possible values denoted as S_\pm . In the first column, we show the simulation results that both the F atoms are scattered in two channels. In the second one, we show results that F atom is scattered in channel I but not scattered in channel II. The third column contains simulation results that F atom is not scattered in channel I but scattered in channel II. In the last column, we show the simulation results that neither the F atoms are scattered in two channels.

3. Numerical Simulation

In this section, we predict the possible results for the experiment shown in Figure 1. Consider that the F atom pairs in the experiment shown in Figure 1 are prepared initially at bipartite Werner state,^[54] whose density matrix can be written as

$$\rho_W = \begin{pmatrix} \frac{1-p}{4} & 0 & 0 & 0 \\ 0 & \frac{1+p}{4} & \frac{p}{2} & 0 \\ 0 & \frac{p}{2} & \frac{1+p}{4} & 0 \\ 0 & 0 & 0 & \frac{1-p}{4} \end{pmatrix} \quad (10)$$

where $0 \leq p \leq 1$. When $p = 1$, the Werner state yields a pure Bell state, with maximum entanglement in bipartite systems, while if $p = 0$, the Werner state degenerates into a uniformly mixed state whose density matrix is just $\frac{I}{4}$, with I being the identity matrix.

We simulated the experimental results as shown in Figure 3. In the first channel shown in Figure 1b, the F atom goes into scattering chamber together with the HD beams. The collision energy is set around $2.10 \text{ kcal mol}^{-1}$, where the horseshoe shape pattern (see Figure 2b) is observed in certain product distribution. Figure 3a is a scheme of the DCS for the $F(^2P_{1/2,3/2}) + HD(\nu = 0, j = 0)$ reaction. The only product included in this data is the

HF($\nu' = 3$). The data are digitized from ref. [55] by fitting the relevant peaks to gaussian functions. The two DCS curves in this plot represents the two outcomes of the Z-measurement. On the other hand, in another channel shown in Figure 1c, the scattering process corresponds to measurement by $\frac{Z+X}{\sqrt{2}}$ operator. For simplicity, here we assume that the DCS for $|\Phi_R^\pm\rangle$ are well described as shown in Figure 3b, where $|\Phi_R^\pm\rangle$ are eigenstates of $\frac{Z+X}{\sqrt{2}}$. Due to lack of experimental results, the corresponding DCS in Figure 3b are randomly generated patterns. It must be emphasized that the overall assertion in this report will remain unchanged for any other pattern as well as long as the DCS curves for the $|\Phi_R^\pm\rangle$ have sufficiently different support as is the case in Figure 3b.

Numerical simulations predict the experimental results as shown in Figure 3c–e, for Werner states with various p values, $p = 0, 0.707, 1$. The variable θ in these subfigures is the scattering angle of product HF($\nu' = 3$), and Γ is the direct measurement result with two possible values denoted as S_\pm which are either the Z-measurement result in chamber I with observed value of ± 1 or $\frac{Z+X}{\sqrt{2}}$ value in chamber II with observed value of ± 1 . The vertical axis in each subfigure represent the frequency of F atom pairs with a certain measurement results. For example in the 1st column of Figure 3c, the vertical axis shows the count of F atom pairs, one of which have been detected by direct Z-measurement in chamber I and have also scattered a HF($\nu' = 3$) within a neighborhood of θ_1 (say) while the other have been detected in chamber II by $\frac{Z+X}{\sqrt{2}}$ and have concomitantly scattered a HF($\nu' = 3$) within a neighborhood of θ_2 (say). The second column shows the count of F atom pairs one of which have scattered a HF($\nu' = 3$) in channel I within a given neighborhood of θ and the other have resulted in a $\frac{Z+X}{\sqrt{2}}$ measurement of ± 1 . Similar interpretation can be constructed for the horizontal and vertical axes of the third and fourth column in the said figure. All axes in columns of Figures 3d and 3e have similar meaning as these but simulated for Werner states of the initial F atom pairs with different p values. For the case of each of the p values, we simulated the experiment 100 000 times, and assume that the probability of single F atoms to be scattered is 0.5, regardless to its initial states. For $p = 0.707$ which is the onset of an entanglement and $p = 1.0$ which corresponds to a Bell state, we do see the expected anti-correlation in Figures 3d and 3e especially in the 4th column. Such features are absent for $p = 0$, which corresponds to a maximally mixed state. Even though Werner states with various p values might lead to such extreme differences, it could always be challenging to read out these features directly from these counts. Alternatively, we can estimate the test statistics formed by quantum correlations with the CHSH inequality for continuous variables shown in Equation (9) which we discuss next.

Alternatively, we can estimate the test statistics formed by quantum correlations with the CHSH inequality for continuous variables shown in Equation (9). Test statistics for various p values are shown in Figure 4, where the red line indicates the theoretical prediction, and the blue dots represent simulation results. When $p \geq 0.707$, it is expected to observe violation of the CHSH inequality; in other words, the test statistic is greater than 2, which guarantees the existence of entanglement.

In brief, the existence of entanglement can be detected with the generalized CHSH inequality Equation (9), while the spe-

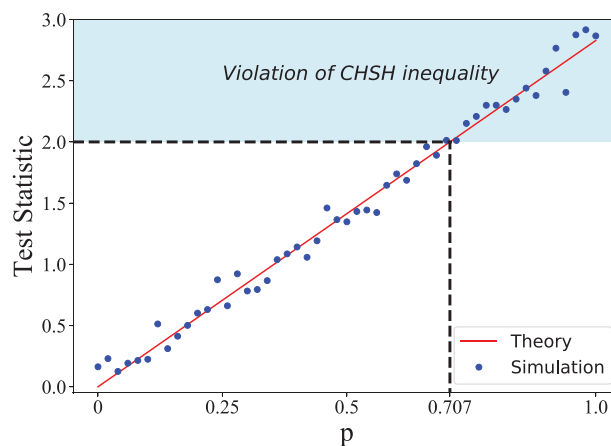


Figure 4. Test statistics for various p values. The red line indicates the theoretical prediction, and the blue dots represent simulation results. When $p \geq 1/\sqrt{2}$, it is expected to observe violation of the CHSH inequality, which guarantees the existence of entanglement. The light blue area indicates the violation of the CHSH inequality.

cial patterns in DSC indicates the necessity for the inclusion of spin–orbit characteristics (see Figure 2b). With the experimental implementation shown in Figure 1, the test statistic can be estimated based on the collected data from two channels with four measurements and the frequency of F atom pairs detected satisfying the possible outcomes of the measurements can be plotted as shown in Figure 3c (or Figure 3d,e). Violation of the generalized CHSH inequality in the count statistics guarantees the existence of entanglement. On the other hand, we need to focus on the DCSs of certain products. Observation of the horseshoe shape patterns like Figure 2b in product HF($\nu' = 2, j' = 5$) indicates the full spin–orbit characteristics. Observation of the horseshoe shape patterns, along with violation of the CHSH inequality, indicates that the existence of entanglement between the initial F atom pairs has little influence on the spin–orbit characteristics, so that the six-state still works as before. In contrast, another possible result is that the CHSH inequality is violated; meanwhile, there is no horseshoe shape patterns in the forward-scattering of $\nu' = 2$ products. If so, we need to admit that the potential energy surface (PES) changes with the entanglement between F atom pairs. For example, patterns like Figure 2a in the forward-scattering suggest that the PES reduces to Equation (2), which can be described with the simple two state model. Additionally, entanglement might be vulnerable under the collisions. If so, we need to apply lower collision energy, ensuring that entanglement will not be broken in the reactions.

4. Conclusion

In this paper, we propose an experiment to study the possible statistical correlation between entanglement and features associated with spin–orbit coupling, where both the existence of entanglement and the spin–orbit characteristics can be detected simultaneously. Particularly, we propose an implementation of the experiment based on the F + HD reaction. The existence of entanglement can be guaranteed from the violation of generalized CHSH inequality for continuous variables which can be

ascertained from the frequency of F atom pair distribution, while the special patterns in DSC from the product HF distribution would mandate the necessity for the inclusion of spin-orbit characteristics. We further numerically simulated the possible experimental results, pointing out the key features for various realizable outputs. Under the assumption that the DCS curves for two of the possible direct measurements $\frac{Z+X}{\sqrt{2}}$ have nearly disjointed supports (see Figure 3b). With advancement in experimental controls, the marriage of such studies which hope to illustrate hidden correlations between initial reactant molecules (atoms) and known geometrical features of product distribution can be undertaken and even possibly exploited as a formidable resource.

Acknowledgements

The authors acknowledge funding by the U.S. Department of Energy (Office of Basic Energy Sciences) under Award No. DE-SC0019215, and the National Science Foundation under Award No. 1955907.

Conflict of Interest

The authors declare no conflict of interest.

Data Availability Statement

The data that support the findings of this study are available from the corresponding author upon reasonable request.

Keywords

quantum entanglement, quantum molecular scattering, quantum simulation, spin-orbit coupling

Received: July 18, 2021

Revised: September 16, 2021

Published online:

- [1] S. Kais, K. B. Whaley, A. R. Dinner, S. A. Rice, *Quantum Information and Computation for Chemistry*, John Wiley & Sons, New York **2014**.
- [2] J. Preskill, *arXiv preprint arXiv:2106.10522*, **2021**.
- [3] R. Ursin, F. Tiefenbacher, T. Schmitt-Manderbach, H. Weier, T. Scheidl, M. Lindenthal, B. Blauensteiner, T. Jennewein, J. Perdigues, P. Trojek, B. Oemer, M. Fuerst, M. Meyenburg, J. Rarity, Z. Sodnik, C. Barbieri, H. Weinfurter, A. Zeilinger, *Nat. Phys.* **2007**, *3*, 481.
- [4] W. Zhang, D.-S. Ding, Y.-B. Sheng, L. Zhou, B.-S. Shi, G.-C. Guo, *Phys. Rev. Lett.* **2017**, *118*, 220501.
- [5] C. L. Degen, F. Reinhard, P. Cappellaro, *Rev. Mod. Phys.* **2017**, *89*, 035002.
- [6] S. Pirandola, B. R. Bardhan, T. Gehring, C. Weedbrook, S. Lloyd, *Nat. Photonics* **2018**, *12*, 724.
- [7] V. Giovannetti, S. Lloyd, L. Maccone, *Phys. Rev. Lett.* **2006**, *96*, 010401.
- [8] M. Karra, K. Sharma, B. Friedrich, S. Kais, D. Herschbach, *J. Chem. Phys.* **2016**, *144*, 094301.
- [9] Y. Cao, J. Romero, J. P. Olson, M. Degroote, P. D. Johnson, M. Kieferová, I. D. Kivlichan, T. Menke, B. Peropadre, N. P. Sawaya, S. Sim, L. Veis, A. Aspuru-Guzik, *Chem. Rev.* **2019**, *119*, 10856.
- [10] A. D. King, J. Raymond, T. Lanting, S. V. Isakov, M. Mohseni, G. Poulin-Lamarre, S. Ejtemaee, W. Bernoudy, I. Ozfidan, A. Y. Smirnov, M. Reis, F. Altomare, M. Babcock, C. Baron, A. J. Berkley, K. Boothby, P. I. Bunyk, H. Christiani, C. Enderud, B. Evert, R. Harris, E. Hoskinson, S. Huang, K. Jooya, A. Khodabandelou, N. Ladizinsky, R. Li, P. A. Lott, A. J. R. MacDonald, D. Marsden, et al., *Nat. Commun.* **2021**, *12*, 1113.
- [11] S. Kais, *Adv. Chem. Phys.* **2007**, *134*, 493.
- [12] R. Blatt, D. Wineland, *Nature* **2008**, *453*, 1008.
- [13] M. Bayer, P. Hawrylak, K. Hinzer, S. Fafard, M. Korkusinski, Z. Wasilewski, O. Stern, A. Forchel, *Science* **2001**, *291*, 451.
- [14] S. Shankar, M. Hatridge, Z. Leghtas, K. Sliwa, A. Narla, U. Vool, S. M. Girvin, L. Frunzio, M. Mirrahimi, M. H. Devoret, *Nature* **2013**, *504*, 419.
- [15] X.-L. Wang, L.-K. Chen, W. Li, H.-L. Huang, C. Liu, C. Chen, Y.-H. Luo, Z.-E. Su, D. Wu, Z.-D. Li, H. Lu, Y. Hu, X. Jiang, C.-Z. Peng, L. Li, N.-L. Liu, Y.-A. Chen, C.-Y. Lu, J.-W. Pan, *Phys. Rev. Lett.* **2016**, *117*, 210502.
- [16] Z. Huang, S. Kais, *Chem. Phys. Lett.* **2005**, *413*, 1.
- [17] Y. Lin, D. R. Leibbrandt, D. Leibfried, C.-w. Chou, *Nature* **2020**, *581*, 273.
- [18] Z. Huang, S. Kais, *Phys. Rev. A* **2006**, *73*, 022339.
- [19] S. Oh, Z. Huang, U. Peskin, S. Kais, *Phys. Rev. A* **2008**, *78*, 062106.
- [20] J. Zhu, S. Kais, A. Aspuru-Guzik, S. Rodrigues, B. Brock, P. J. Love, *J. Chem. Phys.* **2012**, *137*, 074112.
- [21] J. A. Pauls, Y. Zhang, G. P. Berman, S. Kais, *Phys. Rev. E* **2013**, *87*, 062704.
- [22] D. B. Blasing, J. Pérez-Ríos, Y. Yan, S. Dutta, C.-H. Li, Q. Zhou, Y. P. Chen, *Phys. Rev. Lett.* **2018**, *121*, 073202.
- [23] P. G. Jambrina, D. Herráez-Aguilar, F. J. Aoz, M. Sneha, J. Jankunas, R. N. Zare, *Nat. Chem.* **2015**, *7*, 661.
- [24] S. S. Kale, Y. P. Chen, S. Kais, *arXiv preprint arXiv:2107.05441*, **2021**.
- [25] R. Zare, A. Schmeltekopf, W. Harrop, D. Albritton, *J. Mol. Spectrosc.* **1973**, *46*, 37.
- [26] J. C. Tully, *J. Chem. Phys.* **1974**, *60*, 3042.
- [27] D. Herschbach, in *25th Int. Congress of Pure and Applied Chemistry*, Elsevier, New York **1977**, pp. 61–73.
- [28] D. R. Herschbach, *Faraday Discuss. Chem. Soc.* **1987**, *84*, 465.
- [29] R. D. Levine, *Molecular Reaction Dynamics*, Cambridge University Press, **2009**.
- [30] G. C. Schatz, J. M. Bowman, A. Kuppermann, *J. Chem. Phys.* **1973**, *58*, 4023.
- [31] S.-F. Wu, B. Johnson, R. Levine, *Mol. Phys.* **1973**, *25*, 839.
- [32] D. G. Truhlar (Ed.), *Resonances in Electron-Molecule Scattering, Van Der Waals Complexes, and Reactive Chemical Dynamics*, ACS Symposium Series, American Chemical Society, **1984**.
- [33] F. Fernández-Alonso, R. N. Zare, *Annu. Rev. Phys. Chem.* **2002**, *53*, 67.
- [34] J. C. Polanyi, A. H. Zewail, *Acc. Chem. Res.* **1995**, *28*, 119.
- [35] R. T. Skodje, D. Skouteris, D. E. Manolopoulos, S.-H. Lee, F. Dong, K. Liu, *Phys. Rev. Lett.* **2000**, *85*, 1206.
- [36] D. Neumark, A. Wodtke, G. Robinson, C. Hayden, Y.-T. Lee, *Phys. Rev. Lett.* **1984**, *53*, 226.
- [37] F. J. Aoz, L. Bañares, V. J. Herrero, V. S. Rábanos, K. Stark, H.-J. Werner, *Chem. Phys. Lett.* **1994**, *223*, 215.
- [38] J. F. Castillo, D. E. Manolopoulos, K. Stark, H.-J. Werner, *J. Chem. Phys.* **1996**, *104*, 6531.
- [39] D. E. Manolopoulos, K. Stark, H.-J. Werner, D. W. Arnold, S. E. Bradforth, D. M. Neumark, *Science* **1993**, *262*, 1852.
- [40] C. L. Russell, D. E. Manolopoulos, *Chem. Phys. Lett.* **1996**, *256*, 465.
- [41] J. B. Kim, M. L. Weichman, T. F. Sjolander, D. M. Neumark, J. Ktos, M. H. Alexander, D. E. Manolopoulos, *Science* **2015**, *349*, 510.
- [42] T. Yang, L. Huang, C. Xiao, J. Chen, T. Wang, D. Dai, F. Lique, M. H. Alexander, Z. Sun, D. H. Zhang, X. Yang, D. M. Neumark, *Nat. Chem.* **2019**, *11*, 744.

- [43] M. Qiu, Z. Ren, L. Che, D. Dai, S. A. Harich, X. Wang, X. Yang, C. Xu, D. Xie, M. Gustafsson, R. T. Skodje, Z. Sun, D. H. Zhang, *Science* **2006**, 311, 1440.
- [44] C.-x. Xu, D.-q. Xie, D.-h. Zhang, *Chin. J. Chem. Phys.* **2006**, 19, 96.
- [45] Z. Ren, L. Che, M. Qiu, X. Wang, W. Dong, D. Dai, X. Wang, X. Yang, Z. Sun, B. Fu, S.-Y. Lee, X. Xu, D. H. Zhang, *Proc. Natl. Acad. Sci. USA* **2008**, 105, 12662.
- [46] W. Chen, R. Wang, D. Yuan, H. Zhao, C. Luo, Y. Tan, S. Li, D. H. Zhang, X. Wang, Z. Sun, X. Yan, *Science* **2021**, 371, 936.
- [47] V. Zeman, M. Shapiro, P. Brumer, *Phys. Rev. Lett.* **2004**, 92, 133204.
- [48] J. Gong, M. Shapiro, P. Brumer, *J. Chem. Phys.* **2003**, 118, 2626.
- [49] D. Yuan, S. Yu, W. Chen, J. Sang, C. Luo, T. Wang, X. Xu, P. Casavecchia, X. Wang, Z. Sun, D. H. Zhang, X. Yang, *Nat. Chem.* **2018**, 10, 653.
- [50] M. H. Alexander, D. E. Manolopoulos, H.-J. Werner, *J. Chem. Phys.* **2000**, 113, 11084.
- [51] M. H. Alexander, G. Capecchi, H.-J. Werner, *Science* **2002**, 296, 715.
- [52] A. Aspect, P. Grangier, G. Roger, *Phys. Rev. Lett.* **1982**, 49, 91.
- [53] J. Li, S. Kais, *Sci. Adv.* **2019**, 5, eaax5283.
- [54] R. F. Werner, *Phys. Rev. A* **1989**, 40, 4277.
- [55] S.-H. Lee, F. Dong, K. Liu, *Faraday Discuss.* **2004**, 127, 49.